Polymer Coating for Li-Metal Anode in Polyethylene Oxide-Based Electrolyte Batteries

Urban Košir, Alen Vizintin, Elena Tchernychova, Gregor Kapun, Matteo Gastaldi, Alia Jouhara, Margaud Lecuyer, Claudio Gerbaldi, Miran Gaberšček, Robert Dominko, and Sara Drvarič Talian*

The push to use metallic lithium-based batteries motivates a shift toward the use of solid polymer electrolytes. To improve the ionic conductivity values of such electrolytes, liquid additives (plasticizers) are usually added. However, the improvement in conductivity comes at the expense of a deterioration of the anode–electrolyte interface, resulting in poorer electrochemical cell performance. In this study, the use of a polymer coating consisting of polyethylene oxide, LiTFSI, and LiNO$_3$ is proposed. The coating shows improved electrochemical performance and stability, delayed cell failure and a more uniform distribution of Li deposits. These improvements are attributed to the increased stability of the solid electrolyte interphase, which is confirmed by using a combination of electrochemical impedance spectroscopy, scanning electron microscopy, and X-ray photoelectron spectroscopy. In contrast, it is found that the interphase in uncoated Li electrodes is likely affected by continuous reactions with the plasticizer, further confirming the need to use such protective coatings to achieve long-term operation in practical solid-state Li metal batteries.

1. Introduction

Lithium-ion batteries (LIB) have established themselves as the primary electrochemical energy storage system for portable electronic devices, grid storage, and electric transportation applications.[1,2] While different cathode materials are employed in current LIB designs, they universally rely on graphite-based anodes. Despite offering a safe and reliable solution with a theoretical specific capacity of 372 mAh g^{-1}, graphite anodes represent a fundamental limitation to the energy density of state-of-the-art LIB.[3] Metallic lithium (Li) is an attractive alternative due to its high theoretical specific capacity of 3,860 mAh g^{-1}. However, the use of Li metal anodes introduces several challenges, which contribute to active material loss, low coulombic efficiency, and severe safety concerns due to the unstable interphase and formation of dendrites that can cause short circuits.[4–7] To address these challenges, solid-state polymer electrolytes have emerged as a promising alternative to reactive liquid electrolytes.[8,9] Among them, the semi-crystalline polymer polyethylene oxide (PEO) has been extensively studied due to its ability to solvate large quantities of Li salts, as well as its cost-effectiveness and inherent safety. However, PEO-based electrolytes exhibit limited ionic conductivity in its crystalline form at temperatures below 60 °C, requiring the use of liquid plasticizers for lower temperature applications.[10] While plasticizers enhance conductivity, they also promote unwanted side reactions with lithium, deteriorating the interfacial stability at the Li–electrolyte interface.[3]

A viable strategy to mitigate these interfacial challenges is to engineer the electrode surface before it contacts the electrolyte. This can be achieved through the application of thin coatings compatible with lithium metal, a technique well explored for liquid electrolyte systems, where coatings primarily serve as interlayers that stabilize lithium deposition.[5,11–16] However, for solid-state polymer electrolytes, research on lithium metal coatings remains relatively scarce. Beyond stabilizing the interface, these coatings must also possess sufficient lithium-ion

U. Košir, A. Vizintin, E. Tchernychova, G. Kapun, M. Gaberšček, R. Dominko, S. Drvarič Talian
Department of materials chemistry
National Institute of Chemistry
Hajdrihova 19, 1000 Ljubljana, Slovenia
E-mail: sara.drvarictalian@ki.si

U. Košir, M. Gaberšček, R. Dominko
Faculty of chemistry and chemical technology
University of Ljubljana
Večna pot 113, 1000 Ljubljana, Slovenia

M. Gastaldi, C. Gerbaldi
GAME Lab
Department of Applied Science and Technology (DISAT)
Politecnico di Torino
Corso Duca degli Abruzzi 24, 10129 Torino, Italy

M. Gastaldi, C. Gerbaldi
National Reference Center for Electrochemical Energy Storage (GISEL) - INSTM Via G.
Giusti 9, 50121 Firenze, Italy

A. Jouhara, M. Lecuyer
Blue Solutions
Odet, Ergué Gaberic, QUIMPER CEDEX 8 29556, France

R. Dominko
ALISTORE - European Research Institute, CNRS FR 3104
15 Rue Baudelocque, Amiens Cedex 80039, France

Batteries & Supercaps

Research Article
doi.org/10.1002/batt.202500402

Chemistry Europe
European Chemical
Societies Publishing

conductivity to allow for efficient ion transport.[17] Common fabrication methods to produce such coatings include drop casting,[16] wet casting,[18] solid-phase passivation,[19] or development of thin polymer-based interlayers.[20] Among these approaches, solution casting offers a scalable fabrication route, with the solvent selection crucial to preventing adverse reactions with metallic lithium. Tetrahydrofuran (THF) is typically used due to its compatibility with metallic lithium and ease of evaporation.[16,18] Additionally, this method of coating facilitates the incorporation of additives, such as $LiNO_3$, which has been shown to enhance the performance of PEO-based polymer electrolytes.[21–23] Although such strategies can enhance battery performance, accurately assessing their impact remains challenging, as solid-state cells are difficult to characterize *ex-situ* without compromising interfacial integrity and thus require more complex approaches, such as characterization techniques utilizing cryogenic conditions.[24,25]

Herein, we report a polymer-based coating for lithium metal anode tailored for use with PEO-based electrolytes incorporating tetraglyme as a plasticizer[26] with the aim of increasing stability and lifetime of polymer electrolyte-based lithium metal batteries. Furthermore, we investigate the impact of the coating on the interfacial and transport properties of the battery cell using galvanostatic cycling, electrochemical impedance spectroscopy (EIS), scanning electron microscopy (SEM), X-ray photoelectron spectroscopy (XPS), and cryogenic plasma-focused ion beam (PFIB).

2. Experimental Section

2.1. Preparation of Solid Polymer Electrolyte (SPE)

The preparation of SPE was adapted from Porcarelli, L. et al.[26] Initially, 0.75 g of benzophenone (Sigma–Aldrich, 99%, CAS 119-61−9) was weighed into a vial and heated to 50°C to melt the crystals. Subsequently, 3.875 g of tetraglyme (TEGDME, E-Lyte Innovations GmbH, CAS 143-24−8, dried with molecular sieves 4 Å for 2 weeks before use) was added to the vial using a glass pipette. A magnetic stir bar was then introduced, and the solution was stirred on a magnetic stirrer. After few minutes, 1.5 g of lithium bis(trifluoromethanesulfonyl)imide (LiTFSI, Sigma–Aldrich 99.99%, CAS 90,076-65−6) salt was added, and stirring continued for another hour until complete dissolution of the salt was achieved. Throughout this process, the vial was wrapped in aluminum foil to prevent light exposure, as benzophenone acts as a photoinitiator. Next, the solution was transferred into a glass beaker, and the stir bar was removed. Temperature was then increased to 60 °C, and 3.875 g of polyethylene oxide (PEO, Sigma–Aldrich, CAS 25,322-68−3, $M_v = 200,000$) was gradually added while continuously stirring with a metallic spatula. At this stage, a viscous mixture formed. To facilitate mixing, the mixture was heated and stirred four times, with reheating between each step to reduce viscosity. During reheating, the beaker remained covered with aluminum foil to prevent light exposure. After thorough mixing, the material was allowed to cool, forming a wax-like solid (Figure S1a, Supporting Information). The total mass of the prepared material was 10.0 g, with a weight composition of 38.75,

38.75, 15, and 7.5% in PEO, TEGDME, LiTFSI, and benzophenone, respectively. The material was then divided into smaller portions (1.125 g each) and placed between two polypropylene (PP) foils with 100 μm spacers to facilitate hot pressing into a membrane-like shape. All preparation steps were conducted inside an Ar-filled MBRAUN Unilab glovebox, where oxygen and water levels were maintained below 0.5 ppm. To preserve an inert environment during hot pressing, the PP foils containing the material were sealed inside an Ar-filled plastic bag (Figure S1b, Supporting Information). The hot press was preheated to 70 °C. The sealed bag was placed between the press plates and initially subjected to light pressure ($\approx$1 bar) for 5 min to soften the SPE material. The pressure was then increased to 15 bar for 10 min to shape the material into a circular membrane with a thickness defined by the inserted spacer. In the final step, the pressed membranes were rapidly transferred to a DYMAX UV-curing machine (ECE 5000, 320–450 nm of emission), where they were irradiated from both sides for 3 min at a 40 mW cm^{-2}. The resulting material was a semi-transparent membrane PEO + G4 (Figure S1c, Supporting Information), which could be safely transferred back into the glovebox for further processing.

2.2. Coating Preparation and Cell Assembly

The preparation of the polymer-based coating solution was conducted inside an MBRAUN glovebox. Initially, 0.476 g of LiTFSI (Solvay, dried under vacuum at 140 °C overnight) and 0.048 g of $LiNO_3$ (Merck, dried under vacuum at 100 °C overnight) were weighed into a glass vial, followed by the addition of 10 mL of tetrahydrofuran (THF, Honeywell, 99.9%). Before use, THF solvent was dried with 4 Å molecular sieves for 3 days, refluxed for one day with K/Na alloy (3/1 wt.) and then distilled. The amount of water in the solvent was determined with Karl Fischer titration (<5 ppm). The solution was stirred inside a closed vial using a magnetic stirrer inside the glovebox until complete dissolution of the salts was achieved. Subsequently, 1.375 g of PEO (Sumitomo, Grade 1L, dried under vacuum at 50 °C overnight) was added to the mixture. After 1 h, the temperature of the magnetic stirrer was increased to 65 °C, and stirring was continued in a closed vial until the solution became transparent ($\approx$ 4 h). The mixture was then allowed to cool to room temperature while stirring was maintained overnight.

Lithium foil (60 μm thick, provided by Blue Solutions) was cut into smaller sections (4 × 10 cm). No surface scratching was performed on the prepared Li substrates. The coating solution was applied to the Li foil using a manual film applicator, with the initial casting thickness set to 15 μm (**Figure 1**a). Following the casting procedure, the coated Li foils were transferred onto a glass plate, where they were left to dry for 2 days and then cut into multiple squares (2 × 2 cm). These squares were then used to punch out lithium electrodes for battery cell assembly.

For symmetrical cell testing (lithium|electrolyte|lithium), an electrode stack was assembled, consisting of two lithium electrodes (coated or uncoated) separated by a 100 μm thick PEO + G4 electrolyte. The lithium electrodes were circular, with a diameter
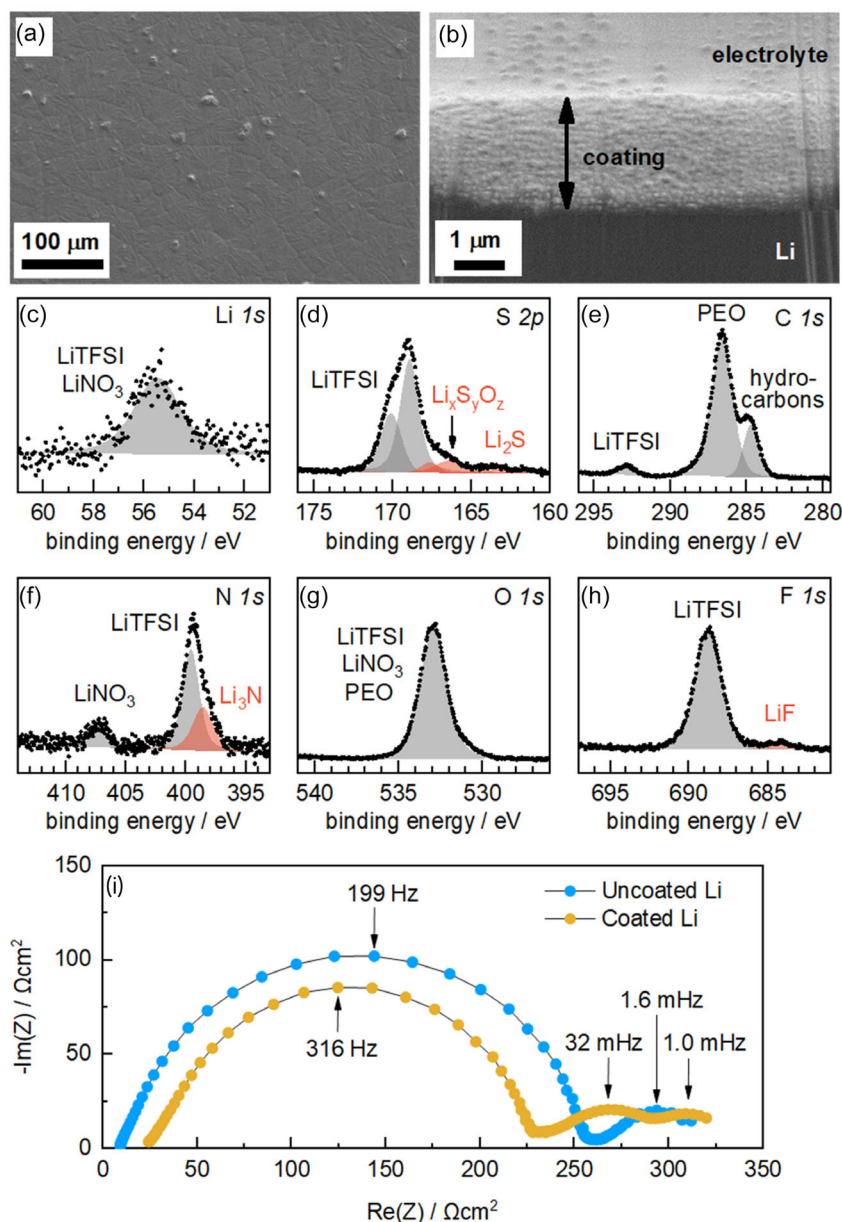
Batteries & Supercaps

Research Article
doi.org/10.1002/batt.202500402

Chemistry Europe
European Chemical
Societies Publishing

Figure 1. a) SEM image of pristine coated Li electrode—top view, b) cross section of coated Li stacked with electrolyte, c–h) Li *1s*, S *2p*, C *1s*, N *1s*, O *1s*, and F *1s* XPS spectra (respectively) of pristine coating and i) comparison of PEIS measurements for Li symmetrical cells using coated lithium (yellow trace) and uncoated lithium (blue trace).

of 16 mm, corresponding to a surface area of 2 cm². Uncoated Li electrodes were used without any additional surface treatment prior to cell assembly. The PEO + G4 electrolyte was cut into circular disks with a diameter of 18 mm, yielding a surface area of 2.5 cm². The stack was compressed with an in-house made weight press, that uses two silicone-protected metallic cylinders. A pressure of 5 bars was used for 5 min at room temperature. Stack was subsequently moved inside a triplex pouch cell (PE 90 μm/Al 10 μm/PET 20 μm) with two Cu contacts inserted into the pouch cell. These cells were heat-sealed using a vacuum sealer inside the glovebox.

A similar procedure was followed for assembling three-electrode cells. In this configuration, two electrolyte layers were used to accommodate a reference electrode (RE) placed between them. The RE consisted of a rectangle-shaped Li wire that was clamped between two copper foils, which served as a current collector to facilitate the connection of the RE to the potentiostat/galvanostat. Schematic illustrations of both cell configurations and the corresponding electrode⊠electrolyte stack dimensions as well as SEM image of the Li RE are provided in Supporting Information note S1.

2.3. Electrochemical Measurements

All electrochemical measurements were conducted at 40 °C inside a BINDER climate chamber using a VMP3e Biologic

Batteries & Supercaps

Research Article
doi.org/10.1002/batt.202500402

Chemistry
Europe

European Chemical
Societies Publishing

Multichannel Potentiostat controlled by EC-Lab software. Electrochemical impedance spectroscopy (EIS) measurements were carried out over a frequency range of 1 MHz–0.5 mHz, with an applied voltage amplitude of 10.0 mV (rms). To determine the lithium-ion transference number (t_{Li+}) of both the electrolyte and the coating, low-frequency EIS was performed on symmetrical cells assembled with varying electrolyte thicknesses and, in a separate set, with varying coating thicknesses. The values for R_{el} (bulk electrolyte/coating resistance) and R_W (real part of the diffusion impedance—Warburg resistance) were obtained from the EIS measurements under open-circuit voltage (OCV) conditions. Using these values and (Equation 1) and (2), the individual resistance contributions R_1 and R_2 were calculated.

$$R_{el} = \frac{R_1 R_2}{R_1 + R_2} \tag{1}$$

$$R_W = R_1 - R_{el} \tag{2}$$

Subsequently, by inserting R_1 and R_2 into (Equation 3), t_{Li+} for the electrolyte and the coating were determined.

$$t_{Li+} = \frac{R_2}{R_1 + R_2} = \frac{R_{el}}{R_1} = \frac{R_{el}}{R_W + R_{el}} \tag{3}$$

When EIS measurements were performed following a galvanostatic cycling procedure, the cells were first rested for 1 h to allow equilibration. Galvanostatic cycling with a time limitation was performed at a current density of 0.1 mA cm^{-2}, with each half-cycle lasting 4 h. For cycle-life evaluation, cells were cycled until failure. However, in three-electrode measurements, the number of cycles was limited to 20. Additionally, tests incorporating an extended half-cycle were conducted at 0.1 mA cm^{-2}, with a time limitation of 48 h.

2.4. Physicochemical Characterization

After completing the electrochemical measurements, the entire pouch cell was immersed in liquid nitrogen for 2 min, then subjected to five cycles of vacuuming/Ar filling inside the glovebox antechamber, each lasting 30 s. The cell was subsequently transferred into the glovebox, where it was opened and disassembled. This procedure enabled easier cell stack disassembly and sample preparation for morphological and physicochemical ex situ characterization.

Scanning electron microscopy (FESEM, SUPRA 35VP, Zeiss) was performed at an accelerating voltage of 2.0–10.0 kV, depending on the sample conductivity. A secondary electron (SE) detector was used to acquire the images. Energy dispersive X-ray spectroscopy (EDS) was performed at 5 kV. Sample transfer was carried out using a custom-built vacuum holder designed to seal the samples on the transfer holder in the glovebox protective atmosphere and open inside the evacuated microscope chamber.

Cryo-plasma-focused ion beam scanning electron microscopy (Cryo-PFIB-SEM) was conducted using a Helios 5 Hydra DualBeam system. Glovebox was used to mount the samples onto a sample stage. Stage was then transferred to a Thermo Fisher Helios 5 Hydra DualBeam system (plasma-focused ion beam scanning electron microscope (PFIB-SEM)) via an inert gas transfer system to avoid air contamination. After that, the stage was cooled to −194 °C in order to prepare the cross sections. Initial digging was performed with focused Xe (+) ions at 30 kV and 0.40 μA. Additionally, polishing was performed with focused Ar (+) ions with lower current (60 nA) in order to reduce the roughness of the cross-sectional image. Morphological images of the surface and cross sections were recorded using a low energy electron beam (1 kV @ 50 pA) and a standard ETD detector in BSE mode.

X-ray photoelectron spectroscopy analysis was done on a Versaprobe 3 AD (Phi, Chanhassen, US) with a monochromatic Al-$K\alpha$1 X-ray (1486.7 eV) excitation source. The samples were placed on copper double-sided tape on the cooling/heating XPS holder inside the glovebox and transferred to the XPS chamber with a transfer tool ensuring protection from the atmosphere. The measurements were conducted in cryo conditions at -140 °C. The spectra were captured over an area of 1×1 mm with a 200 μm spot size. High-resolution spectra were measured at 27 eV pass energy and steps of 0.05 eV. Charge neutralization was used, and the energy scale of the XPS spectra was corrected by shifting the C $1s$ peak of adventitious carbon to a binding energy of 284.8 eV. For the LiTFSI sample, the spectra were shifted according to -CF$_3$ signal in C $1s$ spectra (292.2 eV) and for PEO according to literature reference for both O $1s$ and C $1s$ spectra.[27] The XPS spectra were analyzed with Ulvac-PHI Multipak software, using line background correction.

3. Results and Discussion

Lithium metal-coating composition and thickness were optimized according to the performance of Li‖Li symmetric cells during stripping and plating (Supporting Information note S2). To characterize the chosen coating composition, SEM, XPS, and EIS analyses were performed on pristine-coated electrodes. SEM showed that the surface of Li was uniformly covered with the applied coating (Figure 1a, see also Supporting Information note S3) having a thickness of 3 μm (Figure 1b). XPS analysis of the pristine coating on Li metal shows signals associated with the LiTFSI, LiNO$_3$,-and PEO input materials (gray signals in Figure 1c-h, see also Figure S12, Supporting Information), as well as signals associated with Li$_x$S$_y$O$_z$, Li$_2$S, Li$_3$N, and LiF (marked with red in Figure 1d,f,h), which we attribute to the decomposition of LiTFSI on the Li metal surface after the application of the coating layer to the electrode. Further information on XPS spectra of pristine coating can be found in Supporting Information note S4.

The electrochemical performance of the coating was investigated using a UV-crosslinked solid polymer electrolyte (SPE) composed of PEO, TEGDME, LiTFSI, and benzophenone, following the formulation reported by Porcarelli et al.[26] The influence of the

coating on the Li-SPE interface was studied using electrochemical impedance spectroscopy (Figure 1i). The EIS features were assigned to physicochemical processes based on literature data and model experiments where we varied the electrolyte and coating thickness (Supporting Information note S5). The high frequency (200–350 Hz) arc was attributed to the migration of Li^+ ions through the compact solid electrolyte interphase (SEI). The arc is smaller for the coated cell, and its peak frequency higher compared to the uncoated cell, suggesting improved Li^+ conductivity of the SEI in the coated cell. The coated cell exhibits almost double the electrolyte resistance of the uncoated cell; at lower frequencies, a single arc is observed in the uncoated cell, and two distinct arcs in the coated cell. One arc (1 mHz) was

attributed to diffusion of Li^+ ions through the electrolyte, and the other (32 mHz) to diffusion of Li^+ ions through the polymer coating layer. Both the ionic conductivity ($7·10^{-4}$ S cm^{-1} for electrolyte, $1·10^{-5}$ S cm^{-1} for coating) and transport number (0.19 for electrolyte, 0.15 for coating) appear to be worse for the coating layer, although the impedance is not significantly affected by this because the coating layer is 30-times thinner than the electrolyte. The total resistance of both cells is therefore comparable (*approx.* 320 Ωcm^2 for cells in Figure 1i).

Both the coated and uncoated cells exhibit similar initial overpotentials during galvanostatic stripping and plating in a symmetric Li cell with 0.1 mA cm^{-2} current density (**Figures 2**a,b), which matches our findings from EIS
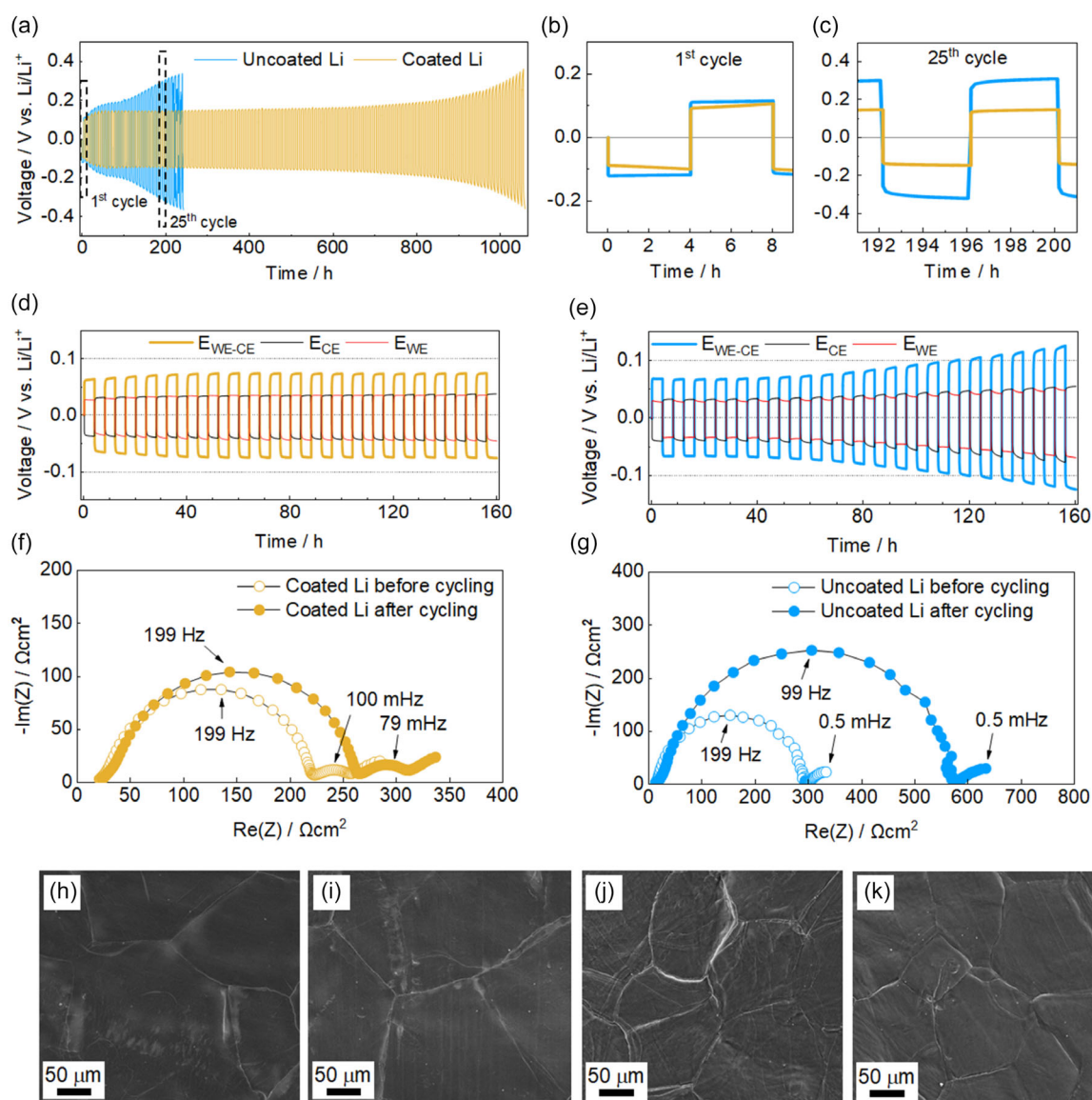

Figure 2. a) Comparison of galvanostatic stripping/plating in symmetric Li cells with time limitations using coated lithium (yellow) and uncoated lithium (blue), b) enlarged view of the 1st cycle, c) enlarged view of the 25th cycle, d) galvanostatic cycling of coated Li in three electrode cell configuration, e) galvanostatic cycling of uncoated Li in three electrode cell configuration, Nyquist plot before/after cycling for coated Li f) and g) uncoated Li cell. h) SEM image of coated working and i) counter electrode, and SEM image of j) uncoated working and k) counter electrode after experiments in (d) and (e).

Batteries & Supercaps

Research Article
doi.org/10.1002/batt.202500402

Chemistry Europe
European Chemical
Societies Publishing

measurements (Figure 1i), where similar total resistance was determined for both cells. A more pronounced increase in overpotential is observed in the uncoated cell over time. In total, the uncoated cell operated for approximately 250 h (roughly 30 cycles) before failing. In contrast, the cell assembled with coated lithium demonstrated significantly longer cycling stability, with a much smaller increase in overpotential throughout the testing period (Figure 2c). It cycled with stable overpotential for roughly 800 h (100 cycles). Then, a gradual increase was observed with each subsequent cycle, resulting in cell failure due to dendrite formation after slightly more than 1000 h of cycling (Figure S17, Supporting Information).

Three-electrode cell experiments on lithium stripping and plating revealed that the increase in overpotential in the uncoated cell primarily originated from the electrode undergoing plating (Figure 2e). In contrast, the coated electrode exhibited significantly lower overpotentials under the same conditions (Figure 2d). One possible explanation for the increased overpotential in the uncoated cell is a loss of contact area between the electrode and the electrolyte, potentially caused by high-surface-area Li deposition. However, this was not supported by SEM analysis, as no evident morphological differences were observed between the coated and uncoated electrodes after 160 h of cycling (Figure 2h-k).

EIS spectra measured on pristine cells and after 160 h of stripping and plating show stable electrolyte resistance values and increase in high-frequency arc associated with SEI resistance (Figure 2f,g). For the uncoated cell, the SEI arc almost doubled from 280 to 555 Ωcm^2, while its peak frequency correspondingly decreased by the same factor (200–100 Hz), keeping the capacitance of the arc a constant 2.9 $\mu F\ cm^{-2}$. The coated cell impedance was more stable with only 20% increase in SEI resistance and a constant 3.5 $\mu F\ cm^{-2}$ capacitance. An increase in SEI resistance (R_{SEI}, (Equation 4)), constant SEI capacitance (C_{SEI}, (Equation 5)) and decrease in peak frequency (f_{peak}, Equation 6) suggest that the geometrical factors (L, thickness of the layer and S, active surface area) remain the same, while the conductivity of the SEI layer (σ) decreases.[28] In (Equation 4) – (6), $\varepsilon, \varepsilon_0,$ and τ, stand for permittivity of the SEI, permittivity of vacuum and the time constant, respectively.

$$R_{SEI} = \sigma \frac{L}{S} \tag{4}$$

$$C_{SEI} = \varepsilon \varepsilon_0 \frac{S}{L} \tag{5}$$

$$f_{peak} = \frac{1}{2\pi\tau} = \frac{1}{2\pi R_{SEI} C_{SEI}} = \frac{1}{2\pi\varepsilon\varepsilon_0\sigma} \tag{6}$$

These changes further disprove the hypothesis of a decrease in the effective contact surface area, since that would induce changes to both the electrolyte resistance and SEI arc capacitance value,

while keeping the SEI arc peak frequency value constant (effectively scaling the EIS spectrum to larger values).[29] On the contrary, the EIS data suggests that the increase in overpotential for the uncoated cell occurs due to changes in SEI chemical composition and, consequently, its ionic conductivity.

To determine the origin of the effective difference in stability between the coated and uncoated Li anode SEI, we conducted XPS analysis of the SEI layer before and after cycling (**Figure 3**, Supporting Information note S6). Because the composition of the polymer coating and polymer electrolyte is very similar (Figure S12, Supporting Information), minimal differences are observed in their initial SEI composition (Figures S18 and S19, Supporting Information). Furthermore, we observe only small changes due to cycling. For the coated cell, we observe a change in the ratio of the components originating from the coating vs. the native SEI (yellow vs gray, Figure 3a–f), which could either be due to changes in SEI composition or difficulties in cell disassembly. We find the latter as more likely: coating layer adhesion on the Li metal anode was so good that we achieved separation of the coating from lithium metal in only approx. 15% of the samples we attempted to disassemble. Even in those cases, we cannot be sure that the coating was fully removed from the surface, which could result in different ratios of the coating vs. native SEI compounds we observed. In our case, the pristine electrode sample had less remaining coating on its surface (lower yellow and higher gray peaks) than the electrode sample after cycling (higher yellow and lower gray peaks).

The electrolyte in the uncoated cell, on the contrary, could be readily removed from the Li electrode. Upon cycling, we observed changes in O 1s spectra attributed to increase in signal due to ROLi compounds (Figure 3k), which are known decomposition products of glymes[30] and PEO.[31] Contrary to the coated electrode analysis, poor adhesion of the electrolyte as well as stable C 1s and F 1s spectra (Figure 3g–l) disprove the possibility of these changes resulting from the variations in the disassembly procedure. The XPS analysis therefore proved that the SEI composition in the uncoated cell changes, while it was not fully conclusive in confirming SEI stability in the coated electrode case (but it is important to note it also did not disprove this option).

Although we successfully separated the electrode and polymer layers by lowering the sample temperature and applying vacuum, we cannot be certain that the probed surface was located at the same depth before and after cycling, or that it corresponded to the electrochemically relevant part of the interface. To more clearly convey this issue, we employed cryo p-FIB to visualize an approximate thickness of the interphase layers, which turned out to be significantly different between the samples. The SEI of the coated electrode was difficult to visualize due to being very thin. We were able to distinguish an approx. 50 nm thick layer between the coating and Li electrode, which had a different contrast (Figure 3m), although we cannot be sure if this is indeed the SEI layer. For the uncoated cell, the electrolyte detached during sample cutting, which is another indirect result of poor electrolyte adhesion. The interfacial layer remaining on the Li electrode was significantly thicker than in the coated cell (roughly 5 μm, Figure 3n) and exhibited porosity as well as a layered

Batteries & Supercaps

Research Article
doi.org/10.1002/batt.202500402

Chemistry Europe
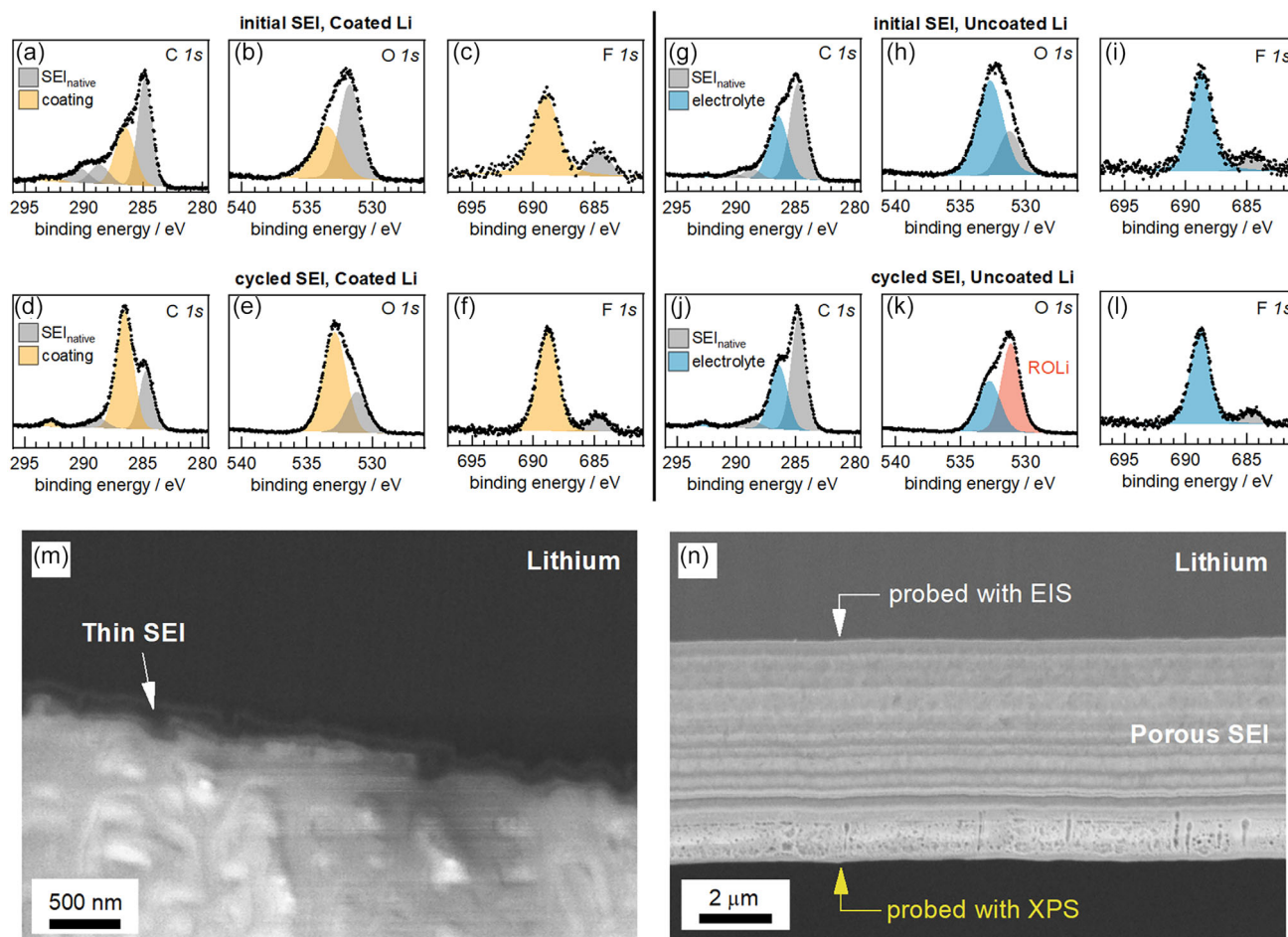European Chemical
Societies Publishing

Figure 3. C 1s, O 1s and F 1s XPS spectra of coated a–c) and uncoated Li metal g–i) electrodes that were in contact with electrolyte for 40 h to perform EIS measurements and spectra after 20 cycles of stripping and plating at 0.1 mA cm^{-1} current density for coated (d–f) and uncoated j–l) electrodes. SEM micrograph of m) Li|coating interphase and n) Li|electrolyte interphase before stripping and plating.

structure. Given this morphology, and considering that XPS is a surface-sensitive technique with a probing depth of only a few nanometers, the XPS spectra primarily reflect the composition of the upper porous layers of the SEI. Due to the substantial SEI thickness, XPS and EIS effectively probe the interface from opposite sides: XPS analyzes the outermost region that was in contact with the electrolyte (see yellow arrow in Figure 3n), while EIS captures the electrochemical response of the inner SEI layers adjacent to the Li metal (see white arrow in Figure 3n).

The structure of the SEI without the coating additionally suggests that the reason for extensive SEI growth might be due to TEGDME solvent addition in the polymer electrolyte, which can help form such structures and, furthermore, wet these porous layers. To explain—if the observed porosity is not filled with liquid electrolyte, we would expect to see very large EIS contribution stemming from the solid-state conduction in the observed layer. As per the discussion in Supporting Information note S5, a typical resistance associated with solid state Li$^+$ ion migration through a 10 nm SEI layer is in the order of a few 100 Ωcm^2. Increasing the thickness by 500x would increase the resistance with the same factor. If the observed porosity is also considered, the expected resistance value increases even further due to a decrease in the effective surface area

(S, (Equation 4)) and increase in thickness (L, (Equation 4)) the ions have to travel. Furthermore, we find it likely that such an SEI was formed through the aid of a liquid component, since a very similar (yet fully solid) coating has not produced the same effect. TEGDME involvement is additionally supported with XPS results showing its common decomposition products (ROLi, Figure 3k).

The conduction of Li$^+$ ions from the bulk of the electrode therefore happens first as solid-state conduction through the compact SEI (the bottom layer, as probed with EIS), then through the liquid portion in the SEI pores (top SEI layer, as probed with XPS) and finally through the conductive pathways of the polymer electrolyte. We expect the resistance due to the transport in the porous portion of the SEI to be a few Ωcm^2 and its peak frequency in the range of a 100 mHz (estimated from typical spectra in Figure S13, Supporting Information). Due to larger contributions from the diffusion of the Li$^+$ ions in the polymer electrolyte in the same frequency region, such contribution is nevertheless not evident from Figure 1i and 2g.

To better understand the increase in overpotentials occurring on the Li electrode during deposition (as observed in the three-electrode cell experiment in Figure 2), we conducted an extended deposition half-cycle on three-electrode cells, lasting
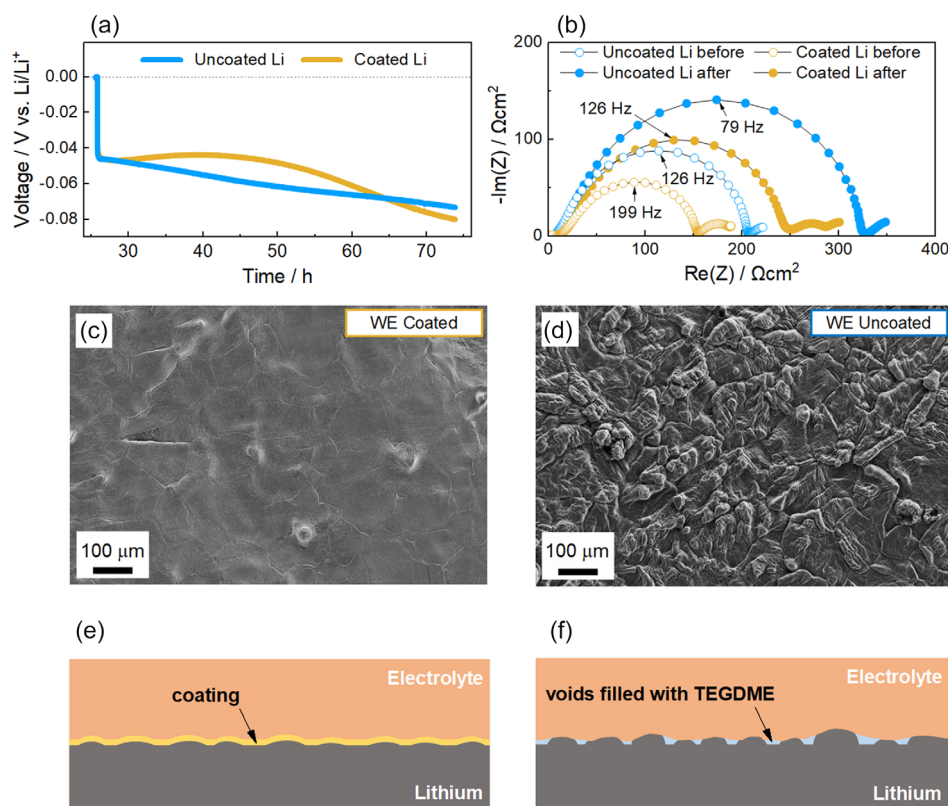
Figure 4. Measurement of an extended galvanostatic half-cycle on a coated lithium (yellow trace) and uncoated lithium (blue trace) symmetrical cell. Plot a) shows the voltage response of the working electrode undergoing lithium deposition. Plot b) compares the PEIS spectra of the same electrode before (hollow circles) and after (filled circles) the galvanostatic half-cycle. Ex-situ SEM images of the coated and uncoated working electrodes that underwent deposition are shown in c) and d), respectively. Coated and uncoated Li electrode–electrolyte interface are schematically presented in e) and f), respectively.

48 h at a current density of $0.1\,\mathrm{mA\,cm^{-2}}$ (**Figure 4**a). This resulted in a charge deposition of $4.8\,\mathrm{mAh\,cm^{-2}}$ (corresponding to a $20\,\mu\mathrm{m}$ increase in the lithium electrode thickness if uniform deposition is assumed). The counter electrode (undergoing stripping) did not exhibit significant differences between the coated and uncoated cells (Figure S20, Supporting Information). However, notable differences were observed on the working electrode. The uncoated electrode displayed a rough morphology, with uneven deposits forming on its surface (Figure 4d). We also observed the electrolyte removed from this surface for indentations which would exactly follow the deposits and indicate good adhesion. The electrolyte surface did not exhibit morphological changes on the same level (Figure S21, Supporting Information), which suggests that voids are formed on the electrode—electrolyte interface. EIS data, on the other hand, again does not support the hypothesis of the loss of contact area. Although the resistance in the uncoated cell increases, the electrolyte resistance and SEI arc capacitance remain close to constant, similar as discussed previously (Figure 4b, (Equation 4) – (6)). A more likely explanation is that the liquid component of the polymer electrolyte (TEGDME) fills the formed voids and enables transport of charge, while the observed increase in resistance is attributed to a reduction in SEI conductivity (Figure 4f).

In contrast, we were not successful in detaching the coating in the *ex-situ* analysis of the plated Li-coated electrode, which indicates good adhesion and a smaller likelihood of void formation on the electrode/coating interface. The coated electrode still shows a certain degree of roughness beneath the coating (Figure 4c), although the excellent adhesion suggests that the coating retains good contact with the Li metal electrode (Figure 4e).

We note that the initial increase and subsequent decrease in overpotential observed in the coated cell (Figure 4a) is not fully addressed within the scope of this work. While preliminary hypotheses suggest that this behavior may result from an interplay between changes in electrode geometry and concentration gradient effects, a comprehensive explanation requires further investigation.

4. Conclusion

This work reported the results of preparation and thorough multi-level characterization of the effect of polymer coating on lithium metal electrode in solid-state Li metal cells with PEO-based polymer electrolyte. The coating demonstrated to improve cycling performance and stability, delay cell failure and reduce uneven Li deposition in symmetric cells. The uncoated electrodes

displayed rough morphology and void formation at the electrode–electrolyte interface, while the coated electrodes maintained a smoother surface, which indicates improved adhesion and reduction in likelihood of void formation. Improved performance and related mechanism were attributed to improved SEI at the Li-coated electrode and related enhanced stability. The extensive SEI growth in uncoated cells is likely due to TEGDME solvent in the polymer electrolyte, which can leach from the structure and contribute to porous SEI formation. The difficulty in disassembling solid-state electrolyte cells and probing the electrochemically relevant interfaces highlights the needs for improvements in characterization methods and techniques. Furthermore, the study suggests the effects of solvent additives in polymer electrolytes need to be closely considered when comparing cell performance. Overall, albeit challenges remain to be solved, through systematically discussing the relationship between structure design, mechanism, and electrochemical properties of the solid electrolyte interphase, we confirm the use of thin coating onto the Li metal electrode as an efficient tool in high-performance crosslinked PEO-based polymer electrolyte solid-state Li metal batteries to promoting their large-scale practical applications under ambient conditions.

Acknowledgments

Conflict of Interest

The authors declare no conflict of interest.

Data Availability Statement

The data that support the findings of this study are available from the corresponding author upon reasonable request.

[1] J. T. Frith, M. J. Lacey, U. Ulissi, *Nat. Commun.* **2023**, *14*, 420.
[2] B. Liu, J. G. Zhang, W. Xu, *Joule* **2018**, *2*, 833.
[3] J. Liu, Z. Bao, Y. Cui, E. J. Dufek, J. B. Goodenough, P. Khalifah, Q. Li, B. Y. Liaw, P. Liu, A. Manthiram, Y. S. Meng, V. R. Subramanian, M. F. Toney, V. V. Viswanathan, M. S. Whittingham, J. Xiao, W. Xu, J. Yang, X. Q. Yang, J. G. Zhang, *Nat. Energy* **2019**, *4*, 180.
[4] D. Lisbona, T. Snee, *Process Saf. Environ. Prot.* **2011**, *89*, 434.
[5] X. B. Cheng, R. Zhang, C. Z. Zhao, Q. Zhang, *Chem. Rev.* **2017**, *117*, 10403.
[6] J. Wang, B. Ge, H. Li, M. Yang, J. Wang, D. Liu, C. Fernandez, X. Chen, Q. Peng, *Chem. Eng. J.* **2021**, *420*, 129739.
[7] K. H. Chen, K. N. Wood, E. Kazyak, W. S. Lepage, A. L. Davis, A. J. Sanchez, N. P. Dasgupta, *J. Mater. Chem. A* **2017**, *5*, 11671.
[8] J. Janek, W. G. Zeier, *Nat. Energy* **2016**, *1*, 16141.
[9] X. Zhang, Y. Yang, Z. Zhou, *Chem. Soc. Rev.* **2020**, *49*, 3040.
[10] J. Mindemark, M. J. Lacey, T. Bowden, D. Brandell, *Prog. Polym. Sci.* **2018**, *81*, 114.
[11] J. Lopez, A. Pei, J. Y. Oh, G. J. N. Wang, Y. Cui, Z. Bao, *J. Am. Chem. Soc.* **2018**, *140*, 11735.
[12] C. Yang, B. Liu, F. Jiang, Y. Zhang, H. Xie, E. Hitz, L. Hu, *Nano Res.* **2017**, *10*, 4256.
[13] Z. Huang, J. C. Lai, S. L. Liao, Z. Yu, Y. Chen, W. Yu, H. Gong, X. Gao, Y. Yang, J. Qin, Y. Cui, Z. Bao, *Nat. Energy* **2023**, *8*, 577.
[14] F. Ding, W. Xu, G. L. Graff, J. Zhang, M. L. Sushko, X. Chen, Y. Shao, M. H. Engelhard, Z. Nie, J. Xiao, X. Liu, P. V. Sushko, J. Liu, J. G. Zhang, *J. Am. Chem. Soc.* **2013**, *135*, 4450.
[15] C. A. Calderón, A. Vizintin, J. Bobnar, D. E. Barraco, E. P. M. Leiva, A. Visintin, S. Fantini, F. Fischer, R. Dominko, *ACS Appl. Energy Mater.* **2020**, *3*, 2020.
[16] M. V. Ordaz, N. Pavlin, M. Gastaldi, C. Gerbaldi, R. Dominko, *ACS Appl. Mater. Interfaces* **2024**, *16*, 68237.
[17] Y. Zhang, T. T. Zuo, J. Popovic, K. Lim, Y. X. Yin, J. Maier, Y. G. Guo, *Mater. Today* **2020**, *33*, 56.
[18] C. Wang, Y. Yang, X. Liu, H. Zhong, H. Xu, Z. Xu, H. Shao, F. Ding, *ACS Appl. Mater. Interfaces* **2017**, *9*, 13694.
[19] Q. Gao, D. Wu, X. Zhu, P. Lu, T. Ma, M. Yang, L. Chen, H. Li, F. Wu, *Nano Energy* **2023**, *117*, 108922.
[20] R. Subramani, M. N. Pham, Y. H. Lin, C. T. Hsieh, Y. L. Lee, J. S. Jan, C. C. Chiu, H. Teng, *Chem. Eng. J.* **2022**, *431*, 133442.
[21] B. Jinisha, K. M. A., M. Manoj, P. Pradeep, J. Jayalekshmi, *Electrochim. Acta* **2017**, *235*, 210.
[22] Z. Zhang, J. Wang, S. Zhang, H. Ying, Z. Zhuang, F. Ma, P. Huang, T. Yang, G. Han, W. Q. Han, *Energy Storage Mater.* **2021**, *43*, 229.
[23] Q. Zhao, P. Chen, S. Li, X. Liu, L. A. Archer, *J. Mater. Chem. A* **2019**, *7*, 7823.
[24] O. Breuer, I. Rozen, N. Leifer, G. Peta, M. Fayena-Greenstein, D. Aurbach, G. Goobes, *J. Electrochem. Soc.* **2024**, *171*, 020532.
[25] M. Yousaf, U. Naseer, A. Imran, Y. Li, W. Aftab, A. Mahmood, N. Mahmood, X. Zhang, P. Gao, Y. Lu, S. Guo, H. Pan, Y. Jiang, *Mater. Today* **2022**, *58*, 238.
[26] L. Porcarelli, C. Gerbaldi, F. Bella, J. R. Nair, *Sci. Rep.* **2016**, *6*, 19892.
[27] P. Louette, F. Bodino, J.-J. Pireaux, *Surf. Sci. Spectra* **2005**, *12*, 59.
[28] M. Gaberšček, S. Pejovnik, *J. Electrochem. Soc.* **1999**, *146*, 933.
[29] S. D. Talian, S. Brutti, M. A. Navarra, J. Moškon, M. Gaberšček, *Energy Storage Mater.* **2024**, *69*, 103413.
[30] A. Kč Lautar, J. Bitenc, T. Rejec, R. Dominko, J. S. Filhol, M. L. Doublet, *J. Am. Chem. Soc.* **2020**, *142*, 5146.
[31] C. Xu, B. Sun, T. Gustafsson, K. Edström, D. Brandell, M. Hahlin, *J. Mater. Chem. A* **2014**, *2*, 7256.